Vacuum 209 (2023) 111752

Contents lists available at ScienceDirect

Vacuum

journal homepage: www.elsevier.com/locate/vacuum

Enhancement on the hardness and oxidation resistance property of TiN/Ag composite films for high temperature applications by addition of Si

Hongbo Ju [a,b,*], Luyao Xu [a], Jing Luan [a], Yaoxiang Geng [a], Junhua Xu [a,**], Lihua Yu [a], Junfeng Yang [c,***], Filipe Fernandes [b,d]

[a] School of Materials Science and Engineering, Jiangsu University of Science and Technology, Mengxi Road 2, Zhenjiang, Jiangsu Province, 212003, China
[b] University of Coimbra, CEMMPRE-Centre for Mechanical Engineering Materials and Processes, Department of Mechanical Engineering, Rua Luís Reis Santos, Coimbra, 3030-788, Portugal
[c] Key Laboratory of Materials Physic, Institute of Solid State Physics, Hefei Institute of Physical Sciences, Chinese Academy of Sciences, Hefei, 230031, China
[d] ISEP—School of Engineering, Polytechnic of Porto, Rua Dr. António Bernardino de Almeida 431, 4200-072, Porto, Portugal

ARTICLE INFO

Handling Editor: Prof. L.G. Hultman

Keywords:
RF magnetron sputtering
$TiN/Ag/Si_3N_4$ films
Hardness
Oxidation resistance

ABSTRACT

Titanium nitride and silver (TiN/Ag) composite films exhibited the excellent self-lubricating properties in a wide temperature range due to the formation of the Ag rich tribolayer in the contact. However, Ag addition usually reduces the hardness and oxidation resistance properties of the films. In this paper, $TiN/Ag/Si_3N_4$ composite films were deposited using RF magnetron co-sputtering system to improve the mechanical and oxidation resistance properties of the TiN/Ag film. XRD and TEM analysis revealed that three-phases could be identified on the $TiN/Ag/Si_3N_4$ films: face-centered cubic (fcc) TiN, fcc-Ag and amorphous Si_3N_4 phases. The hardness of the TiN/Ag film increased from ~16 GPa to ~24 GPa for $TiN/Ag/Si_3N_4$ with 15.3 at.% of Si due to the formation of the nanocomposite structure. The addition of Si allowed a significant improvement on the oxidation resistance temperature, and effectively avoiding of Ag diffusion, and thereby contributing the stability of the hardness of the film after annealing treatment.

1. Introduction

Scientific community and enterprises are seeking for environmentally-friendly solid lubricating materials to replace traditional environmentally harmful lubricating oils, to meet the requirements of low friction and wear resistance reduction in tribological contracts under the severe working conditions is considered as one of the key scientific point in the field of tribology [1–3].

In the last 20 years, a series of self-lubricant hard films were to work at wide-range of temperatures based on the design principle of "adaptive concept" where the tribolayer formed in the contact protects the part from wear [4,5]. For example, C. Baker et al. [6] synthesized the Al_2O_3/DLC/Au/MoS_2 composite films using PVD system and the results indicated that the lubricant phases of DLC, Au and MoS_2 could provide excellent lubricant performances in a wide range of temperatures. Addition of noble metals (such as Au, Ag, etc.) into transitional metal nitride-based (TMN) films also allowed excellent self-lubricating properties. And thereby inducing widely investigation on the TMN based film containing noble metals [7–9]. Nevertheless, the excessive migration of the noble metals in the hard nitride-based films through the grain boundaries at elevated temperatures always led to the premature failure of the films [10–12]. Therefore, the control of the lubricious noble metals' excessive release is the key factor to avoid the premature loss of lubrication at a wide range of temperatures.

Since S. Veperk [13] reported the nanocomposite structure formation in the super-hard Ti–Si–N film system synthesized by physics vapor deposition method and several works have used this concept to improve the mechanical and thermal stability of different film systems. More recently, this kind of film structure design was also proposed to reduce the excessive migration and release of the lubricant phases and/or elements from the interior of the film [14–25], so that the long-term lubricant could be achieved due to the microstructure characteristics

* Corresponding author. School of Materials Science and Engineering, Jiangsu University of Science and Technology, Mengxi Road 2, Zhenjiang, Jiangsu Province, 212003, China.
** Corresponding author.
*** Corresponding author.
E-mail addresses: hbju@just.edu.cn (H. Ju), jhxu@just.edu.cn (J. Xu), jfyang@issp.ac.cn (J. Yang).

https://doi.org/10.1016/j.vacuum.2022.111752
Received 18 September 2022; Received in revised form 13 December 2022; Accepted 13 December 2022
Available online 23 December 2022

of "nano crystal + amorphous". As a matter of fact, based on the above principle of film design, a series of Mo_2N/Cu/SiNx composite thin films were deposited using magnetron sputtering, and results showed that SiN_x can effectively block the growth of Mo_2N grains and make the film exhibit the capsule structure characteristics of "amorphous encapsulated nanocrystals" and the slow release of lubricating phase Cu in high temperature environment is realized and the films has the capability of temperature cycling service [26]. On the other hand, studies concerning the ability of the Ti–Si–N system deposited as either monolithic and multilayer configuration to work as a diffusion barrier to the lubricous Ag elements was recently deeply studied, allowing to conclude that this system successively allow to control/avoid the Ag diffusion from the remaining non oxidized film zone [27–29]. However, to our best knowledge a systematic study on the effect of Si additions on the oxidation resistance of Ti–Si–N–Ag films was not yet reported in the literature. Therefore, a series of TiN/Ag/Si_3N_4 films with different Si content were prepared by using multi-target magnetron sputtering technology, and the microstructure, structure and oxidation properties of the films were studied.

2. Experimental details

2.1. Depositions

A series of TiN/Ag/Si_3N_4 composite films with different Si concentrations were deposited over Si wafer substrate, using radio frequency reactive magnetron sputtering system (the 3D schematic representation of the setup is shown in Fig. 1). The depositions were processed using Ti, Ag and Si targets with a diameter of 75 mm and with a purity of ~99.9%. The substrates were first cleaned ultrasonically in alcohol for 15 min, and acetone for 15 min, and then dried using the hot air before putting into the deposition chamber. The detailed deposition parameters could be summarized as follows: (i) base pressure was below 6.0×10^{-4} Pa and the deposition pressure was 0.3 Pa, (ii) interlayer of Ti was deposited using single Ti target with a power of 150 W for 15 min in pure argon atmosphere, and then Ti and Ag target power was fixed at 200 and 60 W respectively, whereas Si target power was varied between 0 and 150 W to synthesize a series of films with different Si concentration with an interval of 30 W, (iii) argon to nitrogen ratio was 50/1.6 during all the depositions, (iv) no substrate heating and bias voltage were applied, and (v) deposition time was 3 h.

2.2. Films characterization

The elemental chemical composition of the different films was analyzed by an electron probe microanalyzer (EPMA, CAMECA SX-50, France). An average value of three measurements was considered as the elemental compositions. The X-ray diffractometer (XRD, Shimazu-6000, Japan) was applied to investigate the crystalline characterizations of the films. Cu kα irradiation with the voltage and current of 40 kV and 35 mA was used during the measurements. The XRD pattern was processed from 30° to 80° at the scanning step of 2°/min. X-ray photoelectron spectroscopy (XPS, ESCALAB250XI, Thermo Fisher, USA) was used to investigate the chemical state of the elements in the film. The experimental parameters could be summarized as follows:(i) the base pressure during the spectra acquisition was below 2×10^{-9} mbr, (ii) Al target operated at 72 W with the hv of 1486.60 eV was chosen as the excitation source and the Au (4f 7/2, 83.96 eV) was chosen as reference to calibrate, (iii) The recorded spectra include valence band and the total acquisition time was 54.2 s, (iv) The spot size of 400 μm was applied during the measurement, (v) Ion beam etching Ar^+ with a primary energy and the angle of 800 eV and 70°, respectively, was carried out for 30 s to remove the surface contaminants, (vi) The fermi level cut-off occurred at 0 eV from the valence band measurements for the sample according to the Refs. [30–32]. The deconvolution of spectra was performed using the XPS CASA software, in which an adjustment of the peaks was performed using peak fitting with Gaussian–Lorentzian peak shape and Shirley type background subtraction. The hardness of the films was measured using a nano-indentation system (CPX + NHT2 + MST, Swiss) using a constant load of 3 mN for 10 seconds with an indentation depth of below 10% thickness of the films. The onset point of oxidation of the films was evaluated by the thermogravimetric analysis system (TG, DTA, USA). The sample was heated from room temperature to 1000 °C at the heating speed of 15 °C/min in the air.

3. Results and discussion

3.1. Elemental compositions and microstructure

Table 1 illustrates the elemental compositions of the TiN/Ag/Si_3N_4 composite films as a function of Si target power. The Si concentration in the films increases gradually with the increase of Si target power, whilst the Ti and Ag concentrations dropped as expected. However, the N concentration is slight increased, and the O concentration remains approximately constant at ~5 at.%. The Ti/N ratio in the TiN/Ag composite film is ~1.0, but the (Ti + Si)/N ratio gradually decreases with the increase of silicon target power suggesting the formation of sub-stoichiometric films. The increase of the power applied to the Si target contributes to the change of the N concentration, since more metallic atoms are available for the same content of N_2 in the deposition chamber.

Fig. 2 shows the XRD diffraction patterns of the TiN/Ag/Si_3N_4

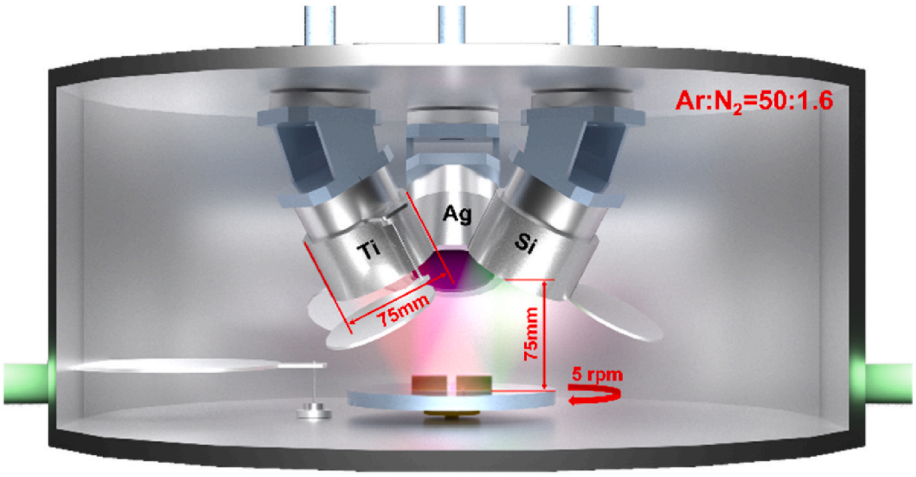

Fig. 1. 3D schematic representation of the deposition system.

Table 1
Elemental chemical composition of the TiN/Ag/Si_3N_4 composite films as a function of the Si target power.

Si target power (W)	Elemental composition (at.%)				
	Ti	Ag	N	Si	O
0	42.6 ± 2.1	11.3 ± 0.6	40.9 ± 2.1	0	5.2 ± 0.3
30	33.5 ± 1.7	10.7 ± 0.5	41.7 ± 2.1	8.7 ± 0.4	5.4 ± 0.3
60	27.9 ± 1.6	9.8 ± 0.5	42.1 ± 2.1	15.3 ± 0.8	4.9 ± 0.3
90	21.9 ± 1.1	9.3 ± 0.5	45.8 ± 2.3	17.2 ± 0.9	5.8 ± 0.3
120	15.4 ± 0.7	8.5 ± 0.4	46.4 ± 2.3	24.6 ± 1.2	5.1 ± 0.3
150	7.9 ± 0.3	7.2 ± 0.4	46.8 ± 2.3	32.5 ± 1.6	5.6 ± 0.3

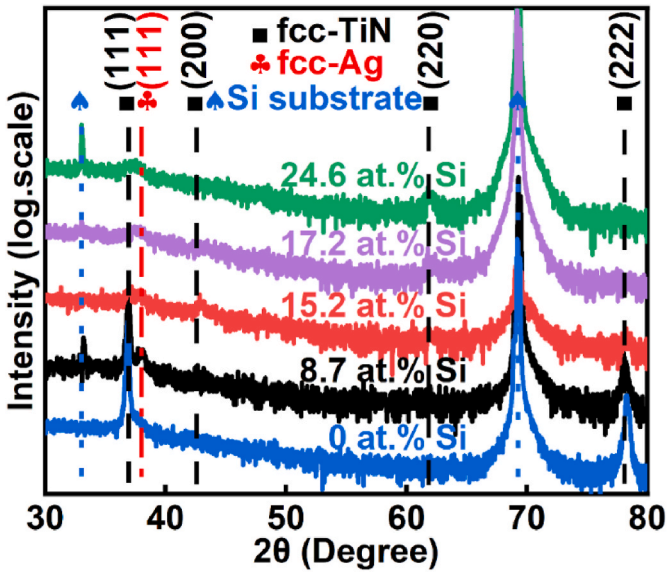

Fig. 2. XRD diffraction patterns of TiN/Ag/Si_3N_4 films with various Si concentrations.

composite films with various Si concentrations. The TiN/Ag film displays double crystallite phases: a face-centered cubic (fcc) TiN phase with diffraction peaks positioned at ~37°, ~38° and ~78° and a fcc-Ag (111) peak located at ~37° [33]. Peaks located at ~34° and ~70° correspond to the signal from the substrate. Addition of Si into the TiN/Ag composite film decreases the intensity of the TiN and Ag diffraction peaks, when 8.7 at% was added. Further increase of Si concentration leads to the formation of amorphous films [34–36]. The amorphous Si–N phase is easily formed during the deposition due to the low enthalpy energy formation of Si–N −850 kJ/mol as compared to TiN (−722.2 kJ/mol) [37]. The amorphous phase which encapsulated the TiN crystallites could prevent the growth of the TiN and Ag grains, contributing to the decrease of the intensity of XRD diffraction peaks related to those phases, and consequently leading to an amorphous structure. This result agrees well with the model of J. Patscheider et al. [38]. Similar results were also reported for the W_2N/SiN_x [39] and Mo_2N/SiN_x [26] film systems with Si additions.

Fig. 3 illustrates the cross-sectional TEM images of the TiN/Ag/Si_3N_4 composite film with a Si concentration of 8.7 at.%. A dense structure with no obvious columnar characteristic could be still detected in Fig. 3 (a). The corresponding selected area electron diffraction (SAED) pattern inset in Fig. 3(a) exhibits a series of diffraction rings corresponding to fcc-TiN and fcc-Ag respectively, in good agreement with the XRD diffraction patterns plotted in Fig. 2. Fig. 3(b) shows the HRTEM image of the film, where crystalline and amorphous regions could be detected. The appearance of two main lattice fringes with the spacing of ~0.2656 and ~0.257 nm, corresponding to fcc-TiN (200) and fcc-Ag (200).

The states of the chemical bonds on the TiN/Ag/Si_3N_4 film with a Si concentration of 8.7 at.% is shown in Fig. 4, representative for all the Si rich films. The original XPS peak is represented by the black continuous line, while the peaks adjusted based on the original peaks are represented by the color lines. The orange color line represents the resultant of the fitting. The survey spectrum of the film is shown in Fig. 4(a), where can be observed that seven elements are detected (Ti, Ag, N, Si, and O). Four peaks with the energy of ~463.8 (Ti–O bond) [40,41], ~461.1 (Ti–N bond) [43], ~458.8 (Ti–O bond) [40], and ~455.0 eV (Ti–N bond) [42,43], are detected in the Ti 2p spectrum in Fig. 4(b). The Ag 3d spectrum (Fig. 4(c)) illustrates two peaks at ~368.6 and ~374.8 eV, which correspond to Ag–Ag bonds in metal silver [44]. As shown in the Si 2p spectrum in Fig. 4(d), two peaks with the energy of ~101.9 and ~103.0 eV, corresponding to the bonds of Si–N in amorphous Si_3N_4 [45] and the Si–O in SiO_2 [46], are detected. Fig. 4(e) illustrates the N 1s XPS spectrum of the film which exhibits the two peaks at ~395.6 (Si–N) [47], ~397.8 (Ti–N) [48–50] respectively. As for the O 1s XPS spectrum in Fig. 4(f), two XPS peaks correspond to the Ti–O [51,52] and Si–O [53] bonds appear.

The XPS results corroborates the XRD and TEM results confirming that fcc-TiN, fcc-Ag and amorphous Si_3N_4 phases coexists in the film's containing Si produced.

3.2. Mechanical and oxidation resistance properties

The hardness of the TiN/Ag/Si_3N_4 films with various Si concentrations is shown in Fig. 5. Reference TiN/Ag film displayed a hardness of ~16 GPa. Additions of Si rises the hardness value to ~24 GPa for the film with the 15.3 at.% Si, and then progressively drops with further increase of Si concentration to a value of ~20 GPa for the film with the 32.5 at.% of Si. The residual stresses measured on the films were in the range of +0.13-+0.09 GPa which does not justify the variations of hardness values. Hence, several other factors can be attribute to the

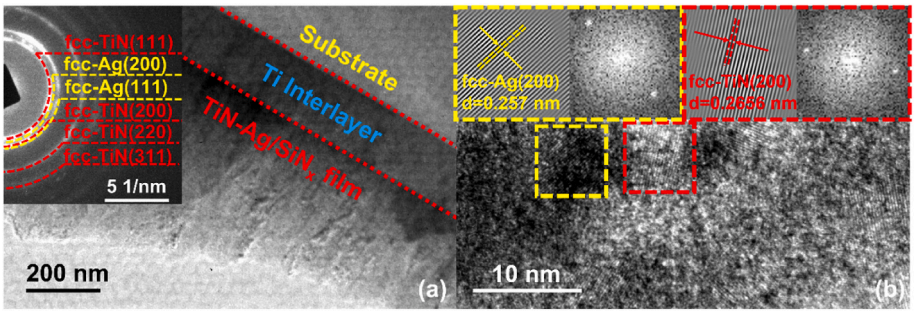

Fig. 3. (a) Cross-sectional TEM and corresponding SAED diffraction pattern of the film with 8.7 at.% of Si, (b) HRTEM images of the different phases.

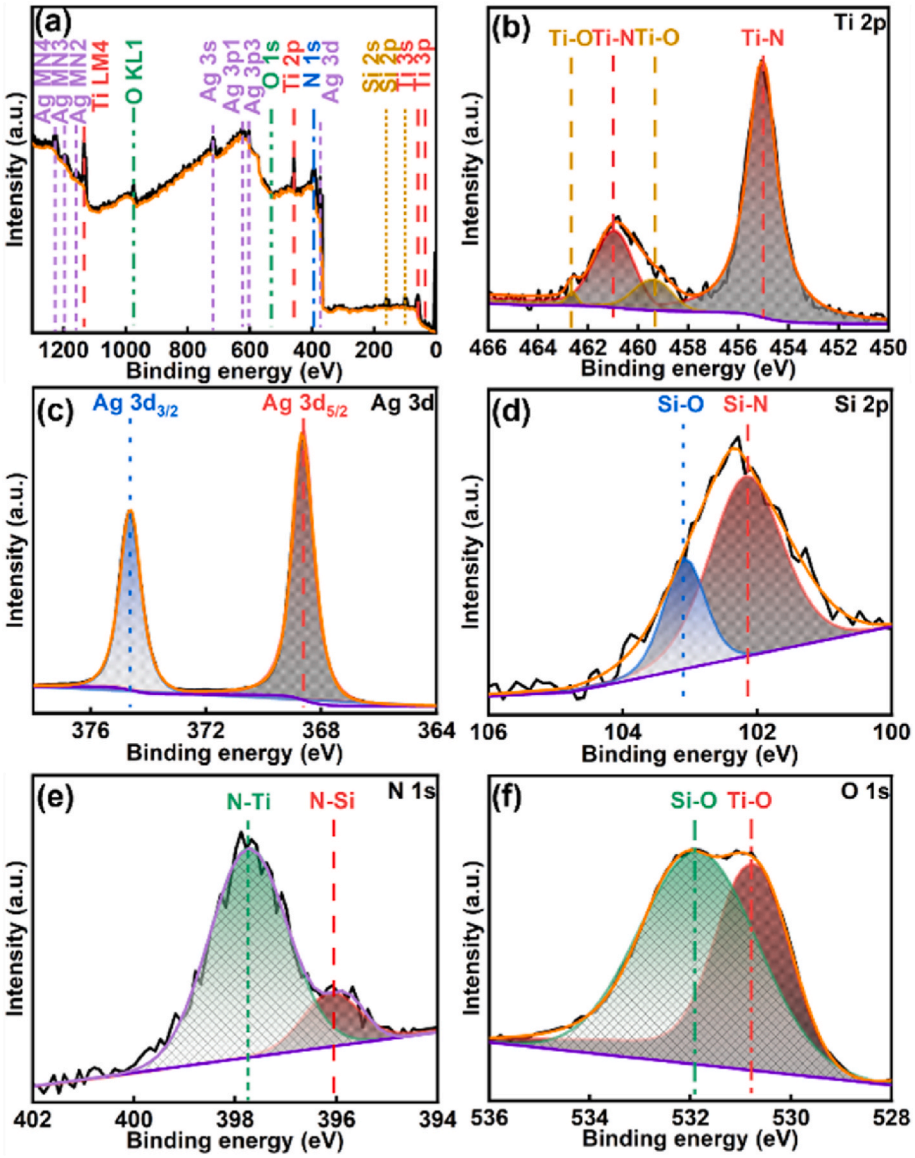

Fig. 4. (a) Survey XPS spectra of TiN/Ag/Si_3N_4 composite film with 8.7 at.% of Si, and high-resolution XPS spectra of: (b) Ti 2p, (c) Ag 3d, (d) Si 2p, (e) N 1s and (f) O 1s.

enhancement of hardness values: (i) The amorphous phase of Si_3N_4 hinders the growth of TiN grains and finally disappears the columnar grains morphologies. This induces the fine grain strengthening and enhances the hardness [54]. (ii) The hardness of the Si_3N_4 film deposited under the same conditions is ~20 GPa, and thereby the formation of the Si_3N_4 phase could increase the hardness of the TiN/Ag film [55]. However, the Si_3N_4 could be considered as the main phase in the composite film and the hardness is close to the one of Si_3N_4 film for the film with a Si concentration above 15.3 at.%. (iii) Heterogeneous interfaces, which could be introduced into the films by formation of amorphous phase of Si_3N_4, act as the strong obstacles to the motions of the dislocation [56–58], and thereby contribute to the enhancement on the hardness based on the principle of interfacial engineering of nanocomposite materials [59–61].

Fig. 6 shows the TG curves of the TiN/Ag/Si_3N_4 films with various Si concentrations. All curves of the films regardless of the Si concentration could be divided into two stages: (i) firstly the relatively weight of the samples exhibits little influence by the testing temperatures, and remains its value of ~100%, (ii) then increases gradually with a further increase of the testing temperatures. The sample exhibits an excellent thermal stability at the first stage, while the oxidation reaction takes place during the second stage. It should be pointed that a slight dropping as a function of testing temperature in the first stage is detected for all samples regardless of silicon concentrations. The thermal denaturation and disappearance of the surface adsorbate induced by the testing temperatures is the reason for this decrease. The onset point of oxidation of the reference TiN/Ag film is ~430 °C. Addition of Si enhances the onset point of oxidation of the films and this point increases for ~780 °C with a Si concentration of 8.7 at.% and to ~990 °C with a Si concentration of 32.5 at.%.

XRD diffraction patterns of reference TiN/Ag and TiN/Ag/Si_3N_4 film with a Si concentration of 8.7 at.% as a function of the annealed temperatures in air are shown in Fig. 7. As shown in Fig. 7(a), the reference TiN/Ag film exhibits an excellent oxidation resistance property after the annealing at 300 °C, since no obvious diffraction peaks corresponding to the oxide-based phases such as TiO_2 are detected in the XRD diffraction pattern. However, the intensity of the diffraction peaks assigned to the fcc-Ag phase becomes stronger with the increase of the annealing temperatures. The grain growth of silver could be induced by the annealing process, and the annealing also reduces the lattice defects of silver phase

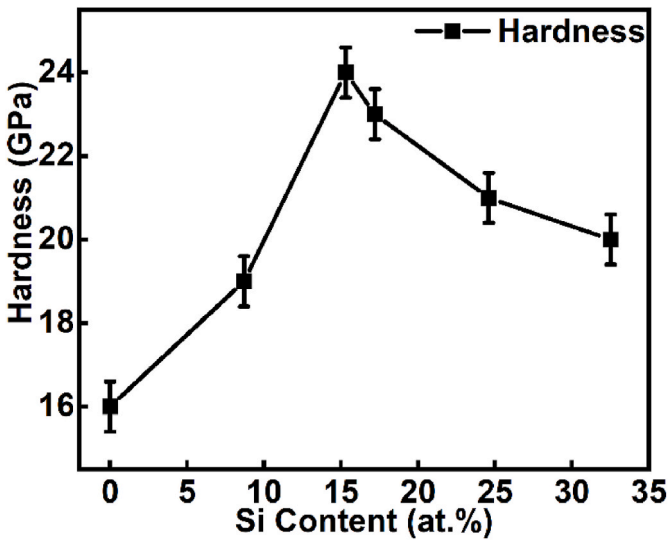

Fig. 5. Hardness of the TiN/Ag/Si_3N_4 films as a function of Si concentration.

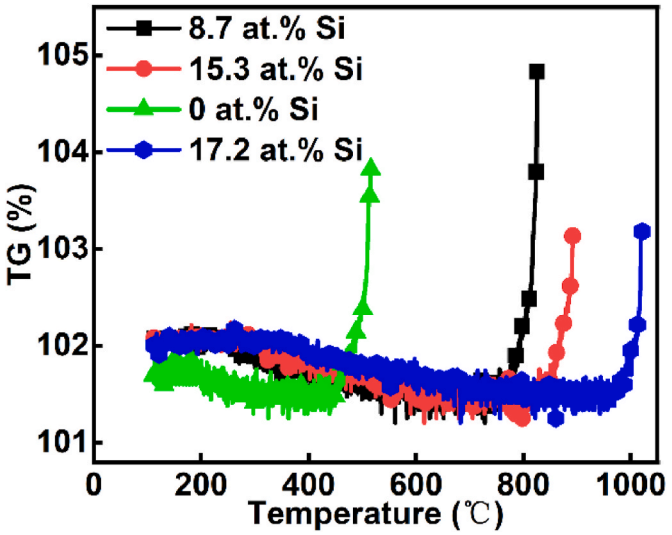

Fig. 6. TG curves of the TiN/Ag/Si_3N_4 films with various Si concentrations.

[62,63]. Therefore, the high quality of Ag crystallographic planes enhances the Bragg diffraction, and contributes to the higher intensity Ag diffraction peaks at this temperature. Moreover, the diffusion of Ag from the inner part to the film surface at elevated temperatures also contributes to the higher intensity of Ag diffraction peaks. A further increase of the annealing temperature (above 400 °C) oxidizes part of the film giving rise to the formation of TiO_2 oxide [64]. For the TiN/Ag/Si_3N_4 sample with a Si concentration of 8.7 at.%, no diffraction peaks assigned to oxides could be detected at 600 °C. At 900 °C a small peak of TiO_2 could be indexed suggesting a little oxidation of the film. Although not detected by XRD due to their amorphous character, SiO_2 phase is also presented in the oxide scale protecting the films from oxidation [65]. The detection of Ag at 900 °C also suggests that Ag diffuses to the surface of the oxidized zone, but for higher temperatures as compared to the reference TiN/Ag film. The higher the Si concentration on the film the lower the diffusion of Ag to the surface. Thus increasing the silver concentration on the films allows the delay of the release of the Ag phase to the surface. Bondarev et al. also confirmed that Ag diffuses from the oxidized zone of the film to the top most zone of the oxidized zone and not from the interior of the non oxidized film [TEM study of the oxidation resistance and diffusion processes in a multilayered TiSiN/TiN (Ag) coating designed for tribological applications [66,67].

The hardness of the TiN/Ag/Si_3N_4 films after different annealing temperatures is shown in Fig. 8. The hardness of the as-deposited films is also shown in this figure for comparison purposes. The 300 °C annealing induces a sharp drop of the hardness of the ternary TiN/Ag film to ~9 GPa. Diffusion of soft Ag to the film surface contributes to this result. However, the hardness of the film after the annealing at 600 °C is slightly enhanced to ~11 GPa and then holds its value with a further increase of the annealing temperature of 900 °C. The enhancement on the hardness could be attributed by the formation of oxide phase of TiO_2.

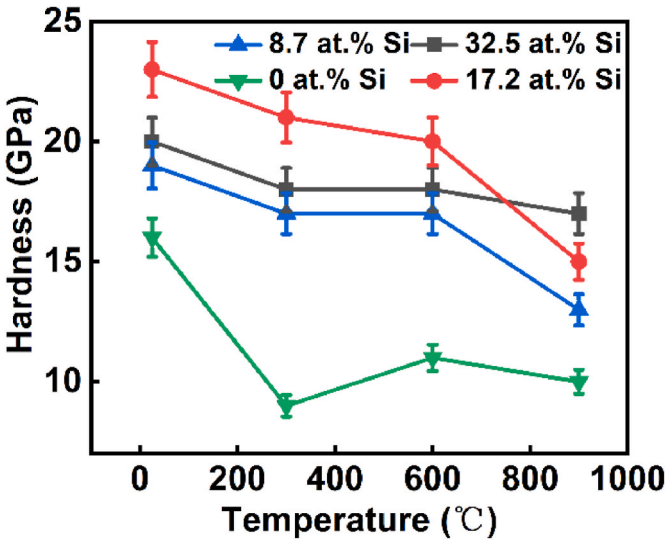

Fig. 8. Hardness of the as-deposited and the annealed TiN/Ag/Si_3N_4 films with different Si concentrations.

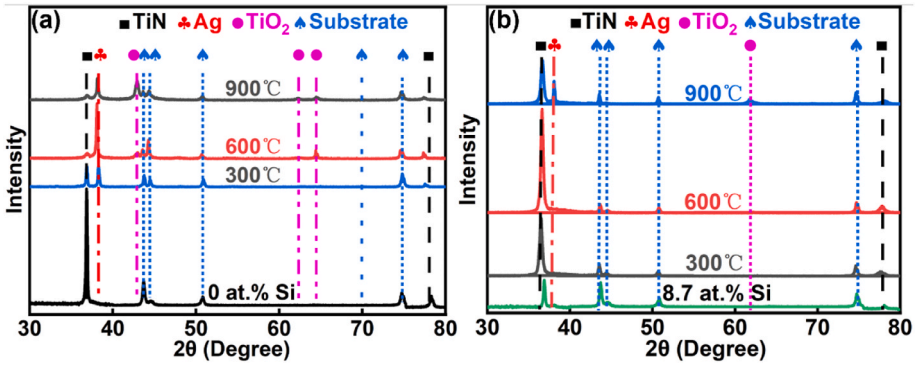

Fig. 7. XRD diffraction patterns of reference TiN/Ag (a) and TiN/Ag/Si_3N_4 with a Si concentration of 8.7 at.% (b) as a function of various annealing temperatures.

As for the TiN/Ag/Si_3N_4 films regardless of Si concentrations, the 300 °C annealing drops the hardness slightly, due to the residual stress release [68] and the grain coarsening [69]. Then their values of the hardness were little influenced by the annealing temperature at 600 °C, since the amorphous phase of Si_3N_4 could avoid the diffusion of Ag and enhance the oxidation resistance temperature. The hardness of the film with the Si concentration of 8.7 and 17.2 at.% was dropped, while the one with a Si concentration of 32.5 at.% holds its hardness, after the annealing at 900 °C. The film with the Si concentration of 8.7 and 17.2 at.% exhibits a poor thermal stability at 900 °C, and the formation of oxide phase of TiO_2 drops the hardness after the 900 °C annealing. But the excellent oxidation resistance property at 900 °C is detected for the film with a Si concentration of 32.5 at.% contributes to the stable value of the hardness.

4. Conclusion

A series of TiN/Ag/Si_3N_4 films with different Si concentrations was synthesized using magnetron sputtering system, and its microstructure, hardness and oxidation resistance properties were investigated. The main conclusions could be summarized as follows:

(1) Three phases, fcc-TiN, fcc-Ag and amorphous Si_3N_4 co-existed in the composite films. Addition of Si into films led to the disappearance of columnar morphology.
(2) Addition of Si into the TiN/Ag composite film enhanced the hardness from ~16 GPa for the film without Si to ~24 GPa for the film with the Si concentration of 15.3 at.%. The grain refinement strengthening and the heterogeneous interfaces induced by the formation of Si_3N_4 contributed to the enhancement on the hardness.
(3) The addition of Si allowed a significant improvement on the oxidation resistance temperature, and effectively avoiding of Ag diffusion, and thereby contributing the stability of the hardness of the film after annealing treatment.

CRediT authorship contribution statement

Hongbo Ju: Writing – review & editing, Writing – original draft, Supervision, Resources, Project administration, Methodology, Investigation, Funding acquisition, Data curation, Conceptualization. **Luyao Xu:** Writing – original draft, Data curation. **Jing Luan:** Writing – review & editing, Methodology, Investigation, Data curation. **Yaoxiang Geng:** Methodology, Data curation. **Junhua Xu:** Supervision, Resources, Project administration, Conceptualization. **Lihua Yu:** Resources, Project administration. **Junfeng Yang:** Resources, Formal analysis. **Filipe Fernandes:** Writing – review & editing, Methodology.

Declaration of competing interest

The authors declare that they have no known competing financial interests or personal relationships that could have appeared to influence the work reported in this paper.

Data availability

Data will be made available on request.

Acknowledgement

Supported by the National Natural Science Foundation of China (51801081, 52071159, 52171071), Portugal National Funds through FCT project (2021.04115.CEECIND), Outstanding University Young Teachers of "Qing Lan Project" of Jiangsu Province, Excellent Talents of "Shenlan Project" of Jiangsu University of Science and Technology. This work is also sponsored by FEDER National funds FCT under the project CEMMPRE – UIDB/00285/2020. MCTool21 project "Manufacturing of cutting tools for the 21st century: from nano-scale material design to numerical process simulation" (reference: POCI-01-0247-FEDER-045940), co-financed by the European Regional Development Fund, through Portugal 2020 (PT2020), and by the Competitiveness and Internationalization Operational Programme (COMPETE 2020).

References

[1] C. Liu, H. Ju, L. Yu, J. Xu, Y. Geng, W. He, J. Jiao, Tribological properties of Mo2N films at elevated temperature, Coatings 9 (11) (2019) 734.
[2] W.J. Huang, M. Sun, W. Wen, J.F. Yang, Z.M. Xie, R. Liu, X.P. Wang, X.B. Wu, C. S. Liu, Q.F. Fang, He2+ irradiation induced microstructure evolution in sub-surface layer of the coarse-grained tungsten accessed by synchrotron GIXRD and GISAXS, Appl. Surf. Sci. 593 (2022) 153461.
[3] C. Liu, H. Ju, J. Xu, L. Yu, Z. Zhao, Y. Geng, Y. Zhao, Influence of copper on the compositions, microstructure and room and elevated temperature tribological properties of the molybdenum nitride film, Surf. Coating. Technol. 395 (2020), 125811.
[4] G. Wang, M. Wen, Y. Wang, J. Qiu, S. Zhang, Y. Li, X. Yang, Y. Si, Q. Song, P. Ren, Tailoring microstructure, mechanical and tribological properties of amorphous CNx films by incorporating Fe, Surf. Coating. Technol. 448 (2022) 128875.
[5] Y. Yao, Y. Wu, Z. Zhang, H. Zhu, M. Hu, K. Xu, Y. Liu, Enhancement of frictional properties of Ni-MoS2 self-lubricating composite coatings by microgroove arrays, Appl. Surf. Sci. (2022), 154635.
[6] C. Baker, J. Hu, A. Voevodin, Preparation of Al2O3/DLC/Au/MoS2 chameleon coatings for space and ambient environments, Surf. Coating. Technol. 201 (7) (2006) 4224–4229.
[7] Z. Chen, L. Qiao, J. Hillairet, Y. Song, V. Turq, P. Wang, R. Laloo, J. Bernard, K. Lu, Y. Cheng, Q. Yang, C. Hernandez, Development and characterization of magnetron sputtered self-lubricating Au-Ni/a-C nano-composite coating on CuCrZr alloy substrate, Appl. Surf. Sci. 492 (2019) 540–549.
[8] H. Ju, P. Jia, J. Xu, L. Yu, I. Asempah, Y. Geng, Crystal structure and high temperature tribological behavior of niobium aluminum nitride films, Materialia 3 (2018) 202–211.
[9] R. Franz, C. Mitterer, Vanadium containing self-adaptive low-friction hard coatings for high-temperature applications: a review, Surf. Coating. Technol. 228 (2013) 1–13.
[10] H. Ju, R. Wang, W. Wang, J. Xu, L. Yu, H. Luo, The microstructure and tribological properties of molybdenum and silicon nitride composite films, Surf. Coating. Technol. 401 (2020), 126238.
[11] X. Jiang, Y. Dai, Q. Xiang, J. Liu, F. Yang, D. Zhang, Microstructure and wear behavior of inductive nitriding layer in Ti–25Nb–3Zr–2Sn–3Mo alloys, Surf. Coating. Technol. 427 (2021), 127835.
[12] G. Utlu, N. Artunç, The effects of grain boundary scattering on electrical resistivity of Ag/NiSi silicide films formed on silicon substrate at 500°C by RTA, Appl. Surf. Sci. 310 (2014) 248–256.
[13] S. Veprek, A. Niederhofer, K. Moto, T. Bolom, H.-D. Männling, P. Nesladek, G. Dollinger, A. Bergmaier, Composition, nanostructure and origin of the ultrahardness in nc-TiN/a-Si3N4/a- and nc-TiSi2 nanocomposites with HV=80 to ≥105 GPa, Surf. Coating. Technol. 133–134 (2000) 152–159.
[14] H. Ju, L. Yu, D. Yu, I. Asempah, J. Xu, Microstructure, mechanical and tribological properties of TiN-Ag films deposited by reactive magnetron sputtering, Vacuum 141 (2017) 82–88.
[15] R. Zhou, H. Ju, S. Liu, Z. Zhao, J. Xu, L. Yu, H. Qian, S. Jia, R. Song, J. Shen, The influences of Ag content on the friction and wear properties of TiCN–Ag films, Vacuum 196 (2022), 110719.
[16] H. Ju, R. Zhou, J. Luan, L. Yu, J. Xu, B. Zuo, J. Yang, Y. Geng, L. Zhao, F. Fernandes, Multilayer Mo2N-Ag/SiNx films for demanding applications: morphology, structure and temperature-cycling tribological properties, Mater. Des. 223 (2022), 111128.
[17] F. Thompson, F. Kustas, K. Coulter, G. Crawford, Dense VSiCN coatings deposited by filament-assisted reactive magnetron sputtering with varying amorphous phase precursor flow rates, Surf. Coating. Technol. 422 (2021), 127507.
[18] C. Liu, H. Ju, P. Han, C. Quan, C. Mo, Y. Zhao, Y. Geng, J. Xu, L. Yu, The influence of carbon content on the microstructure, mechanical and frictional property of chromium carbon nitride composite films, Vacuum 178 (2020), 109368.
[19] H. Ju, D. Yu, J. Xu, L. Yu, Y. Geng, T. Gao, G. Yi, S. Bian, Microstructure, mechanical, and tribological properties of niobium vanadium carbon nitride films, J. Vac. Sci. Technol. 36 (2018), 031511.
[20] M. Mansoorianfar, R. Rahighi, A. Hojjati-Najafabadi, C. Mei, D. Li, Amorphous/crystalline phase control of nanotubular TiO2 membranes via pressure-engineered anodizing, Mater. Des. 198 (2021), 109314.
[21] H. Ju, N. Ding, J. Xu, L. Yu, Y. Geng, F. Ahmed, The tribological behavior of niobium nitride and silver composite films at elevated testing temperatures, Mater. Chem. Phys. 237 (2019), 121840.
[22] H. Ju, P. Jia, J. Xu, L. Yu, Y. Geng, Y. chen, M. Liu, T. Wei, The effects of adding aluminum on crystal structure, mechanical, oxidation resistance, friction and wear properties of nanocomposite vanadium nitride hard films by reactive magnetron sputtering, Mater. Chem. Phys. 215 (2018) 368–375.
[23] S. Hong, J. Park, T. Lee, J. Lim, C. Shin, Y. Park, T. Kim, Variation of poly-Si grain structures under thermal annealing and its effect on the performance of TiN/Al2O3/Si3N4/SiO2/poly-Si capacitors, Appl. Surf. Sci. 477 (2019) 104–110.

[24] H. Ju, R. Zhou, J. Luan, C. Kumar, L. Yu, J. Xu, J. Yang, B. Zhang, F. Fernandes, Tribological performance under different environments of Ti-C-N composite films for marine wear-resistance parts, Int. J. Miner. Metall. Mater. 30 (2023) 144–155, https://doi.org/10.1007/s12613-022-2551-z.
[25] J. Zeng, H. Teng, F. Lu, Electrochemical deposition of barium titanate thin films on TiN/Si substrates, Surf. Coating. Technol. 231 (2013) 297–300.
[26] H. Ju, R. Zhou, S. Liu, L. Yu, J. Xu, Y. Geng, Enhancement of the tribological behavior of self-lubricating nanocomposite Mo2N/Cu films by adding the amorphous SiNx, Surf. Coating. Technol. 423 (2021), 127565.
[27] H. Ju, N. Ding, J. Xu, L. Yu, Y. Geng, F. Ahmed, B. Zuo, L. Shao, The influence of crystal structure and the enhancement of mechanical and frictional properties of titanium nitride film by addition of ruthenium, Appl. Surf. Sci. 489 (2019) 247–254.
[28] F. Findik, Latest progress on tribological properties of industrial materials, Mater. Des. 57 (2014) 218–244.
[29] A. Bondarev, P. Kiryukhantsev-Korneev, E. Levashov, D. Shtansky, Tribological behavior and self-healing functionality of TiNbCN-Ag coatings in wide temperature range, Appl. Surf. Sci. 396 (2017) 110–120.
[30] G. Greczynski, L. Hultman, C 1s peak of adventitious carbon aligns to the vacuum level: dire consequences for material's bonding assignment by photoelectron spectroscopy, Chem. Phys.Chem. 18 (12) (2017) 1507–1512.
[31] G. Greczynski, L. Hultman, The same chemical state of carbon gives rise to two peaks in X-ray photoelectron spectroscopy, Sci. Rep. 11 (2021), 11195.
[32] G. Greczynski, L. Hultman, Compromising science by ignorant instrument calibration—need to revisit half a century of published XPS Data, Angew. Chem. Int. Ed. 59 (13) (2020) 5002–5006.
[33] M. Hu, X. Gao, J. Sun, L. Weng, F. Zhou, W. Liu, The effects of nanoscaled amorphous Si and SiNx protective layers on the atomic oxygen resistant and tribological properties of Ag film, Appl. Surf. Sci. 258 (15) (2012) 5683–5688.
[34] V. Ezhil Selvi, V. William Grips, H. Barshilia, Electrochemical behavior of superhard nanocomposite coatings of TiN/Si3N4 prepared by reactive DC unbalanced magnetron sputtering, Surf. Coating. Technol. 224 (2013) 42–48.
[35] H. Ju, D. Yu, J. Xu, L. Yu, B. Zuo, Y. Geng, T. Huang, L. Shao, L. Ren, C. Du, H. Zhang, H. Mao, Crystal structure and tribological properties of ZrAlMoN composite films deposited by magnetron sputtering, Mater. Chem. Phys. 230 (2019) 347–354.
[36] L. Wang, Y. Huang, Y. Yuan, C. Jia, L. Yang, Microstructure, wear and oxidation resistance of Al-doped Ti–Si3N4 coatings by laser cladding, Surf. Coating. Technol. 429 (2022), 127942.
[37] J. Chen, Y. Wang, W. Gao, D. Wang, S. Chen, J. Luan, A newly designed NiP duplex coating on friction stir welding joint of 6061-T6 aluminum, Surf. Coating. Technol. 448 (2022), 128940.
[38] V. Ivashchenko, S. Veprek, A. Argon, P. Turchi, L. Gorb, F. Hill, J. Leszczynski, First-principles quantum molecular calculations of structural and mechanical properties of TiN/SiNx heterostructures, and the achievable hardness of the nc-TiN/SiNx nanocomposites, Thin Solid Films 578 (2015) 83–92.
[39] H. Ju, S. He, L. Yu, I. Asempah, J. Xu, The improvement of oxidation resistance, mechanical and tribological properties of W2N films by doping silicon, Surf. Coating. Technol. 317 (2017) 158–165.
[40] M. Parlinska-Wojtan, A. Karimi, O. Coddet, T. Cselle, M. Morstein, Characterization of thermally treated TiAlSiN coatings by TEM and nanoindentation, Surf. Coating. Technol. 188–189 (2004) 344–350.
[41] G. Greczynski, L. Hultman, A step-by-step guide to perform x-ray photoelectron spectroscopy, J. Appl. Phys. 132 (2022), 011101.
[42] C. Zou, J. Zhang, W. Xie, L. Shao, L. Guo, D. Fu, Characterization and properties Ti–Al–Si–N nanocomposite coatings prepared by middle frequency magnetron sputtering, Appl. Surf. Sci. 257 (24) (2011) 10373–10378.
[43] H. Ju, D. Yu, L. Yu, N. Ding, J. Xu, X. Zhang, Y. Zheng, L. Yang, X. He, The influence of Ag contents on the microstructure, mechanical and tribological properties of ZrN-Ag films, Vacuum 148 (2018) 54–61.
[44] C. Dang, J. Li, Y. Wang, Y. Yang, Y. Wang, J. Chen, Influence of Ag contents on structure and tribological properties of TiSiN-Ag nanocomposite coatings on Ti–6Al–4V, Appl. Surf. Sci. 394 (2017) 613–624.
[45] K. Zhang, L. Wang, G. Yue, Y. Chen, D. Peng, Z. Qi, Z. Wang, Structure and mechanical properties of TiAlSiN/Si3N4 multilayer coatings, Surf. Coating. Technol. 205 (12) (2011) 3588–3595.
[46] S. Yadav, S. Sahoo, Interface study of thermally driven chemical kinetics involved in Ti/Si3N4 based metal-substrate assembly by X-ray photoelectron spectroscopy, Appl. Surf. Sci. 541 (2021), 148465.
[47] G. Greczynski, L. Hultman, Self-consistent modelling of X-ray photoelectron spectra from air-exposed polycrystalline TiN thin films, Appl. Surf. Sci. 387 (2016) 294–300.
[48] T. Wang, G. Zhang, B. Jiang, Microstructure, mechanical and tribological properties of TiMoN/Si3N4 nano-multilayer films deposited by magnetron sputtering, Appl. Surf. Sci. 326 (2015) 162–167.
[49] C. Tseng, J. Hsieh, W. Wu, S. Chang, C. Chang, Emergence of Ag particles and their effects on the mechanical properties of TaN–Ag nanocomposite thin films, Surf. Coating. Technol. 201 (24) (2007) 9565–9570.
[50] A. Vyas, K. Li, Y. Shen, Influence of deposition conditions on mechanical and tribological properties of nanostructured TiN/CNx multilayer films, Surf. Coating. Technol. 203 (8) (2009) 967–975.
[51] P. Zhang, Z. Cai, W. Xiong, Influence of Si content and growth condition on the microstructure and mechanical properties of Ti–Si–N nanocomposite films, Surf. Coating. Technol. 201 (15) (2007) 6819–6823.
[52] J. Guillot, J. Chappé, O. Heintz, N. Martin, L. Imhoff, J. Takadoum, Phase mixture in MOCVD and reactive sputtering TiOxNy thin films revealed and quantified by XPS factorial analysis, Acta Mater. 54 (11) (2006) 3067–3074.
[53] Y. Zhang, Y. Yang, Y. Zhai, P. Zhang, Effect of negative substrate bias on the microstructure and mechanical properties of Ti–Si–N films deposited by a hybrid filtered cathodic arc and ion beam sputtering technique, Appl. Surf. Sci. 258 (18) (2012) 6897–6901.
[54] H. Ju, J. Xu, Microstructure and tribological properties of NbN-Ag composite films by reactive magnetron sputtering, Appl. Surf. Sci. 355 (2015) 878–883.
[55] T. Soares, C. Aguzzoli, G. Soares, C. Figueroa, I. Baumvol, Physicochemical and mechanical properties of crystalline/amorphous CrN/Si3N4 multilayers, Surf. Coating. Technol. 237 (2013) 170–175.
[56] Y. Xu, L. Li, X. Cai, P. Chu, Hard nanocomposite Ti–Si–N films prepared by DC reactive magnetron sputtering using Ti–Si mosaic target, Surf. Coating. Technol. 201 (15) (2007) 6824–6827.
[57] D. Cavaleiro, A. Cavaleiro, S. Carvalho, F. Fernandes, Oxidation behaviour of TiSiN (Ag) films deposited by high power impulse magnetron sputtering, Thin Solid Films 688 (2019), 137423.
[58] H. Ju, X. He, L. Yu, J. Xu, The microstructure and tribological properties at elevated temperatures of tungsten silicon nitride films, Surf. Coating. Technol. 326 (2017) 255–263.
[59] Y. Ou, X. Ouyang, B. Liao, X. Zhang, S. Zhang, Hard yet tough CrN/Si3N4 multilayer coatings deposited by the combined deep oscillation magnetron sputtering and pulsed dc magnetron sputtering, Appl. Surf. Sci. 502 (2020), 144168.
[60] H. Ju, N. Ding, J. Xu, L. Yu, I. Asempah, J. Xu, G. Yi, B. Ma, Crystal structure and the improvement of the mechanical and tribological properties of tungsten nitride films by addition of titanium, Surf. Coating. Technol. 345 (2018) 132–139.
[61] P. Das, S. Anwar, S. Bajpai, S. Anwar, Structural and mechanical evolution of TiAlSiN nanocomposite coating under influence of Si3N4 power, Surf. Coating. Technol. 307 (2016) 676–682.
[62] M. Nussbaum, M. Yazdi, A. Michau, E. Monsifrot, F. Schuster, H. Maskrot, A. Billard, Mechanical properties and high temperature oxidation resistance of (AlCrTiV)N coatings synthesized by cathodic arc deposition, Surf. Coating. Technol. 434 (2022), 128228.
[63] H. Ju, R. Wang, N. Ding, L. Yu, J. Xu, F. Ahmed, B. Zuo, Y. Geng, Improvement on the oxidation resistance and tribological properties of molybdenum disulfide film by doping nitrogen, Mater. Des. 186 (2020), 108300.
[64] A. Al-Rjoub, A. Cavaleiro, F. Fernandes, Influence of Ag alloying on the morphology, structure, mechanical properties, thermal stability and oxidation resistance of multilayered TiSiN/Ti(Ag)N films, Mater. Des. 192 (2020), 108703.
[65] P. Ondračka, D. Nečas, M. Carette, S. Elisabeth, D. Holec, A. Granier, A. Goullet, L. Zajíčková, M. Richard, Unravelling local environments in mixed TiO2–SiO2 thin films by XPS and ab initio calculations, Appl. Surf. Sci. 510 (2020), 145056.
[66] H. Ju, N. Ding, J. Xu, L. Yu, Y. Geng, Yi Guo, T. Wei, Improvement of tribological properties of niobium nitride films via copper addition, Vacuum 158 (2018) 1–5.
[67] A. Al-Rjoub, A. Cavaleiro, T. Yaqub, M. Evaristo, N. Figueiredo, F. Fernandes, TiAlSiN(Ag) coatings for high temperature applications: the influence of Ag alloying on the morphology, structure, thermal stability and oxidation resistance, Surf. Coating. Technol. 442 (2022), 128087.
[68] H. Ju, L. Yu, S. He, I. Asempah, J. Xu, Y. Hou, The enhancement of fracture toughness and tribological properties of the titanium nitride films by doping yttrium, Surf. Coating. Technol. 321 (2017) 57–63.
[69] D. Cavaleiro, A. Cavaleiro, S. Carvalho, F. Fernandes, Oixation behavior of TiSiN (Ag) films deposited by high power impulse magnetron sputtering, Thin Solid Films 688 (2019), 137423.